Final Report: Silicon Waveguide Mach-Zehnder and Michelson Interferometers

Anthony Reiter (anthony.reiter@infleqtion.com)

Introduction

This proposal report describes the design, simulation, fabrication, and experimental analysis of several integrated interferometric circuits from which we extract the group index of their respective silicon waveguides. Using the course fabrication platform with a fixed 220 nm thick Si waveguide layer, we investigate Mach–Zehnder and Michelson interferometers with varying path length imbalances to study the dependence of free spectral range (FSR) on geometry and polarization. The effective and group indices of quasi-TE and quasi-TM modes are computed using Lumerical MODE and fitted to compact polynomial models for rapid analysis. Simulated transmission spectra from Lumerical INTERCONNECT verify the expected FSR behavior and provide a basis for extracting the group index from experimental measurements. These designs will enable a systematic comparison between simulated and measured group indices, and will provide insight into fabrication tolerances and dispersion in integrated photonic waveguides.

Theory

We start by describing the physics of the Mach-Zehnder and Michelson interferometers, in the context of Si waveguides. Figure 1 shows a schematic of a balanced (i.e. $\Delta L = L_2 - L_1 = 0$) Mach-Zehnder interferometer (MZI), which consists of a single input port, two ideal splitters, and a single output port. We will assume that all paths are lossless and have the same effective index.

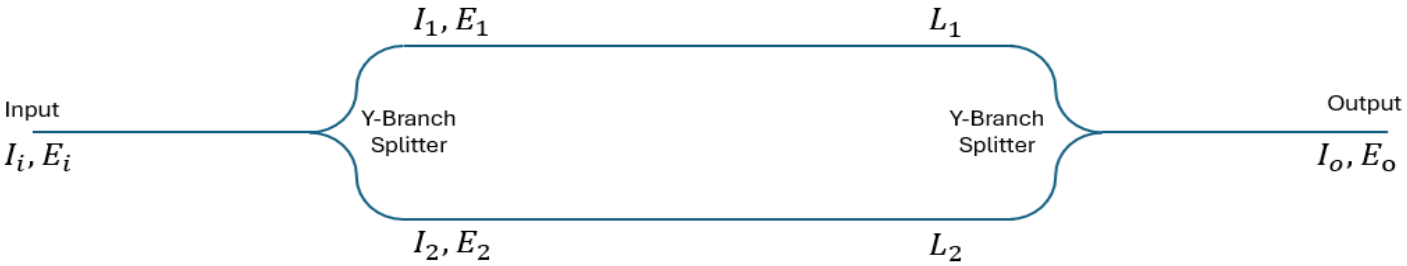

Figure 1: Balanced Mach-Zehnder Interferometer

We consider monochromatic laserlight propagation, where the electric field can be represented by $E = E_0 e^{i(\omega t - \beta z)}$. The propagation direction is z, and the angular frequency and propagation constant are represented by $\omega = 2\pi f = \frac{2\pi c}{\lambda}$ and $\beta = \frac{2\pi n}{\lambda}$, respectively. The effective index of the waveguide, n, is a function of λ.

At the input, we start with an initial intensity, I_i, and electric field amplitude, E_i, where $I_i \propto |E_i|^2$. After the first Y-branch splitter, where the light is split equally into two separate paths, we have $I_1 = \frac{I_i}{2}$, $I_2 = \frac{I_i}{2}$, and $E_1 = \frac{E_i}{\sqrt{2}}$, $E_2 = \frac{E_i}{\sqrt{2}}$. After the second Y-branch splitter, where the light from the two paths is recombined, we have $I_o = I_1 + I_2 = \frac{I_i}{2} + \frac{I_i}{2} = I_i$, and $E_o = \frac{E_1 + E_2}{\sqrt{2}} = E_i$.

Now let's consider the case of the imbalanced (i.e. $\Delta L = L_2 - L_1 \neq 0$) interferometer, shown in Figure 2, where the path lengths between the two Y-branch splitters are unequal.

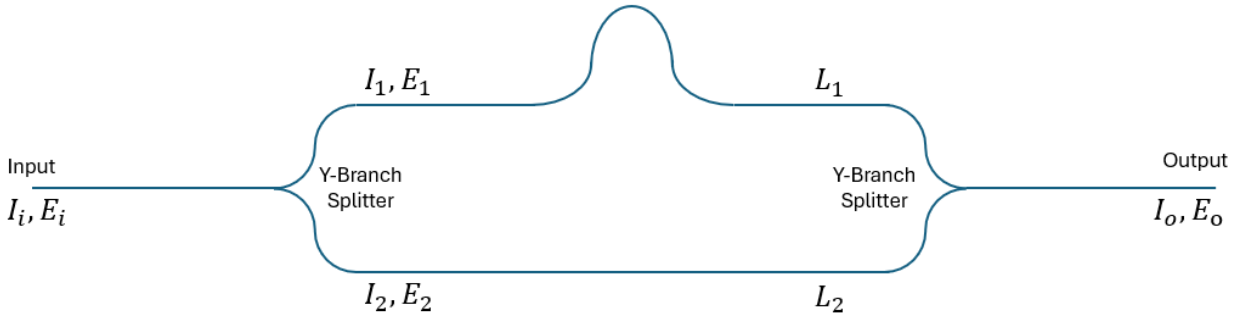

Figure 2: Imbalanced Mach-Zehnder Interferometer

Here, $E_1 = \frac{E_i}{\sqrt{2}} e^{-i\beta L_1}$ and $E_2 = \frac{E_i}{\sqrt{2}} e^{-i\beta L_2}$, which results in $E_o = \frac{E_1 + E_2}{\sqrt{2}} = \frac{E_i}{2}(e^{-i\beta L_1} + e^{-i\beta L_2})$ and $I_o = \frac{I_i}{2}(1 + \cos(\beta \Delta L))$ at the output. Thus, when $\beta \Delta L = \pi$, we have destructive interference, and when $\beta \Delta L = 0$, we have constructive interference. For $\beta \Delta L \neq 0$, the light which is not coupled into the output port is coupled into higher order modes (ex. Second order mode and radiation modes). The MZI transfer function is the ratio of the output and input intensities, given by $\frac{I_o}{I_i} = \frac{1}{2}(1 + \cos(\beta \Delta L))$.

Given the sinusoidal nature of the MZI transfer function, we can see that there are an infinite set of $\beta \Delta L$ values which result in constructive interference. For an imbalanced MZI with a given ΔL, we can calculate the wavelength spacing ($\Delta \lambda$) between these peaks. This spacing is known as the Free Spectral Range (FSR), which is defined as $\Delta \lambda = \frac{\lambda^2}{\Delta L * n_g}$ [ref 1] for the imbalanced MZI, where n_g is the group index. The group index is related to the effective index by $n_g = n - \lambda \frac{dn}{d\lambda}$.

Figure 3 shows a schematic of a balanced Michelson interferometer, which consists of a single input port, an ideal splitter, and two loop mirrors which cause the input light to propagate back in the direction it came. An imbalanced Michelson interferometer can also be considered, either by changing the path length of one of the waveguides between the Y-branch splitter and the loop mirror, or the path

length of one the loop mirrors. The physics is similar to the imbalanced MZI, but the path length difference is accumulated twice, resulting in an FSR of $\Delta\lambda = \frac{\lambda^2}{2*\Delta L*n_g}$. Both interferometer types will be considered in this report.

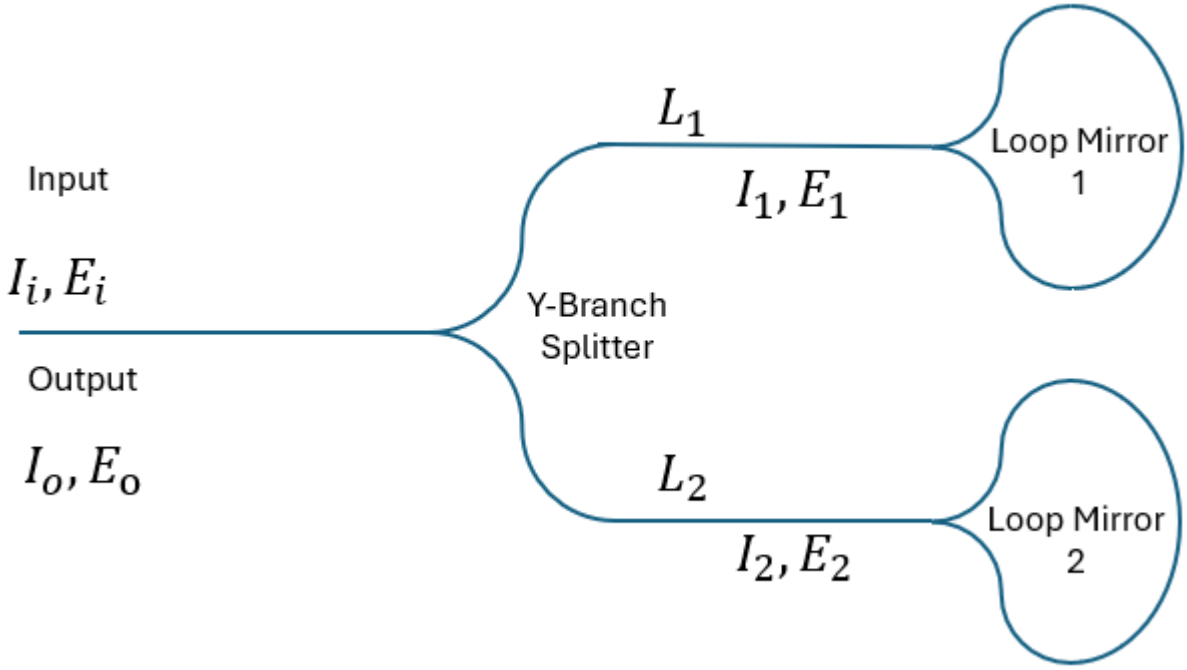

Figure 3: Balanced Michelson Interferometer

Modelling & Simulation

The waveguides investigated in this report are "strip" type, with a Si width and depth of 500nm and 220nm, respectively. Using Lumerical MODE, we can simulate the resulting cross-sectional electric field intensity for both the quasi-TE and quasi-TM modes, as well as the effective and group indices over a given wavelength range. These results are shown in Figures 4, 5, and 6 respectively.

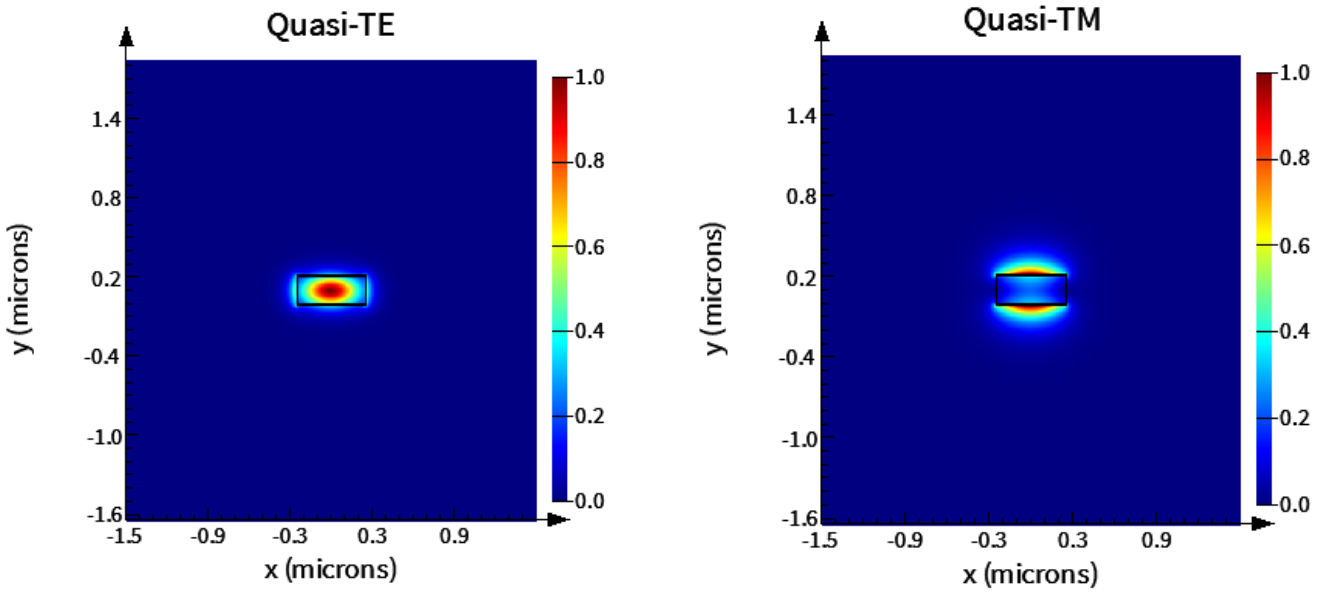

Figure 4: Simulations of electric field for our strip waveguides

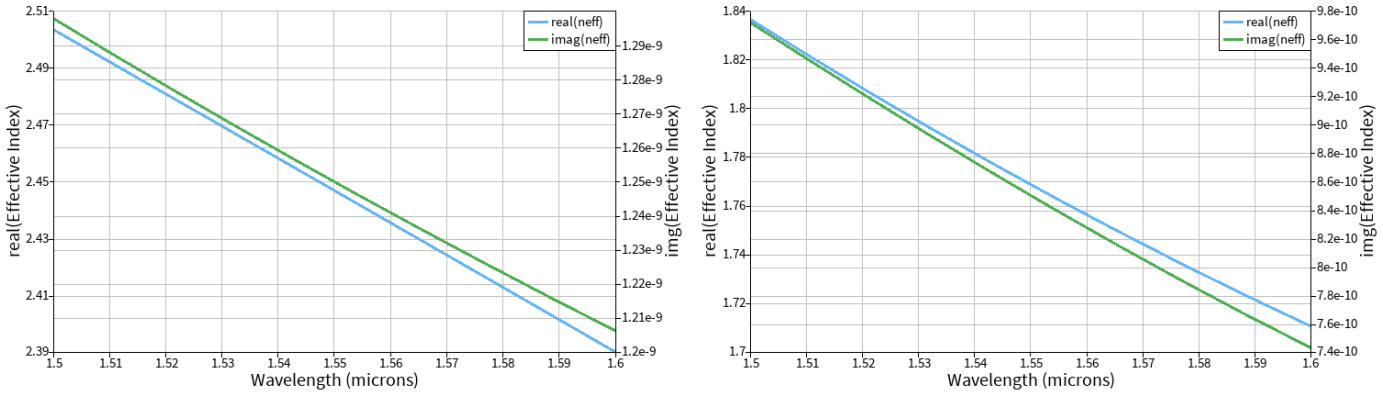

Figure 5: Simulations of n_eff for quasi-TE (left) and quasi-TM (right) modes

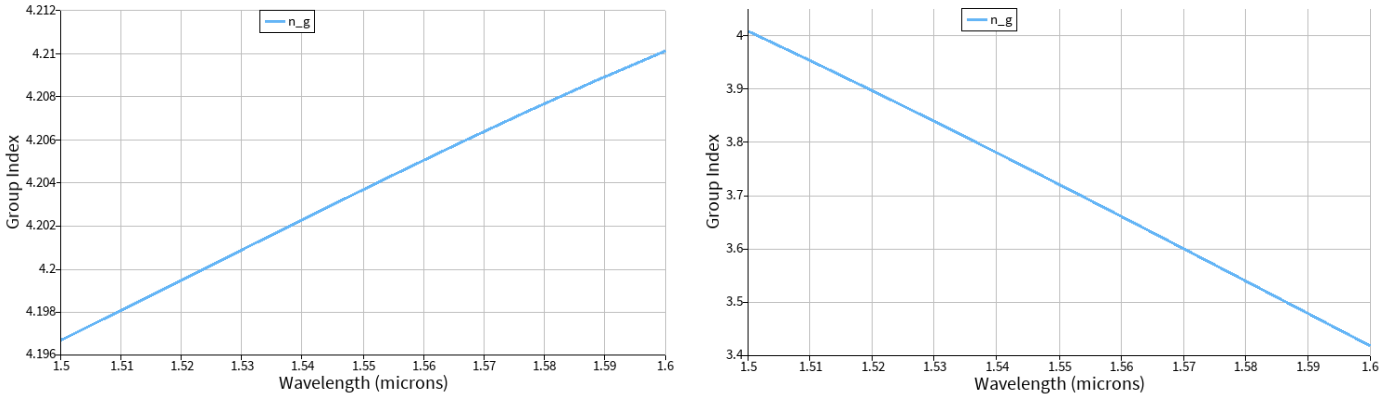

Figure 6: Simulations of n_g for quasi-TE (left) and quasi-TM (right) modes

In order to easily compare our simulated and experimental results, we will refer to the compact model of the waveguide, defined as $n = n_{eff}(\lambda) = n_1 + n_2(\lambda - \lambda_0) + n_3(\lambda - \lambda_0)^2$ [ref 1], which is the result of a Taylor series expansion of $n_{eff}(\lambda)$ around the center wavelength, λ_0. The coefficients in the formula are defined as $n_1 = n_{eff}$, $n_2 = \frac{n_1 - n_g}{\lambda_0}$, and $n_3 = -D * \frac{c}{2\lambda_0}$, where D is the group velocity dispersion. In our case, $\lambda_0 = 1550nm$.

By exporting the simulated n_{eff} vs λ data, and fitting with MATLAB, we obtain the following formulas for n_{eff}:

For the quasi-TE mode: $n_{eff}(\lambda) = 2.45 - 1.13(\lambda - \lambda_0) - 0.04(\lambda - \lambda_0)^2$

For the quasi-TM mode: $n_{eff}(\lambda) = 1.77 - 1.26(\lambda - \lambda_0) - 1.91(\lambda - \lambda_0)^2$

The group indices ($n_g = n_1 - n_2 * \lambda_0$) for the quasi-TE and quasi-TM modes are therefore 4.20 and 3.72, respectively. Using these values, we can calculate the FSR for the following interferometer variations which we will design, fabricate, and test:

Polarization	ΔL (um)	Interferometer Type	FSR @1550nm (nm)
TE	100	MZI	5.72
TE	200	MZI	2.86
TM	100	MZI	6.46
TM	200	MZI	3.23
TE	100	Michelson	2.86
TM	100	Michelson	3.23

Figure 7 shows the model of an MZI constructed within Lumerical INTERCONNECT. An Optical Network Analyzer (ONA) is included in the model in order analyze the performance of the circuit. As seen previously, the MZI includes a Y-branch to evenly split the light into two paths of unequal distance, followed by a second Y-branch for recombining the light. However, grating couplers are also included at the input and output of the MZI, which will enable efficient coupling of light into and out of the waveguides for the real, fabricated circuits. TE and TM optimized grating couplers are available.

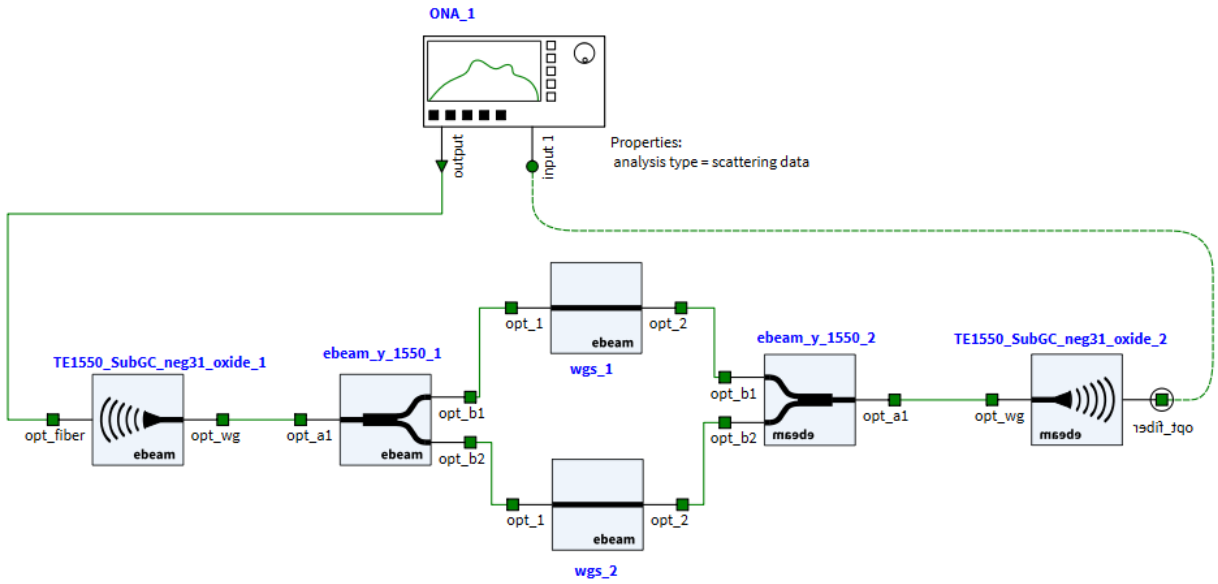

Figure 7: MZI model in Lumerical INTERCONNECT

As an example, we can consider a path length difference of 100um and observe the resulting interferometer spectrum (gain), which is shown in Figure 8.

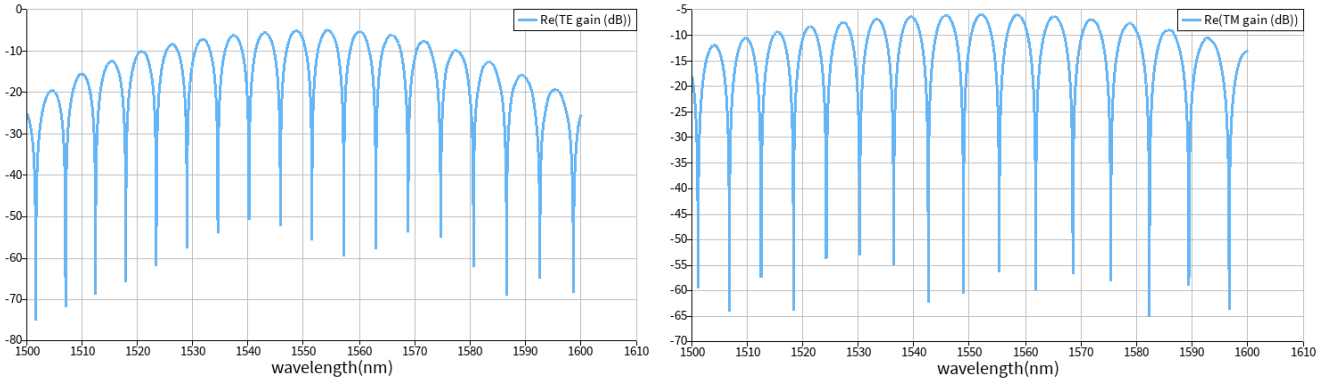

Figure 8: Interferometer spectrum for MZI with TE (left) and TM (right) optimized grating couplers.

An example circuit for a Michelson interferometer and the resulting interferometer spectra are shown in figures 9 and 10, respectively. Here, we implement the use of an adiabatic splitter (optimized for either TE or TM polarization) in order to separate the input and output into two separate ports. The path length difference is again 100um.

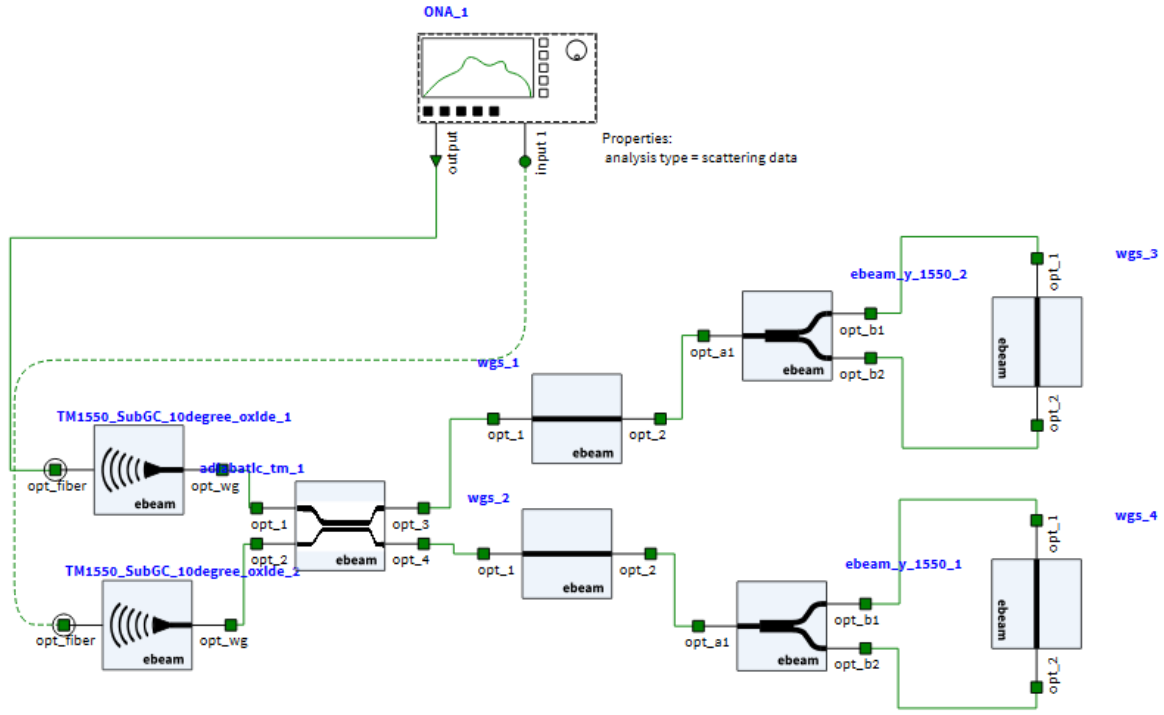

Figure 9: Michelson interferometer model in Lumerical INTERCONNECT

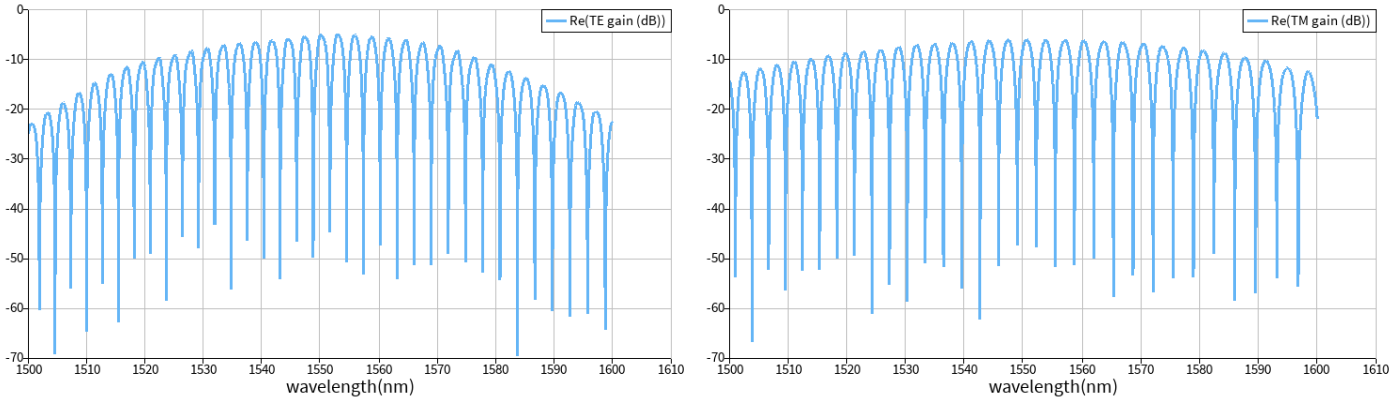

Figure 10: Interferometer spectrum for Michelson interferometer with TE (left) and TM (right) optimized grating couplers and adiabatic splitter.

Fabrication

As with all manufacturing processes, there is some inherent variability in the fabrication process of our interferometers, due to a variety of factors. However, the dominant manufacturing parameter that results in optical component and circuit variation is the top silicon thickness variation [ref 1]. Therefore, we will consider the potential range of effective index, group index, and FSR that result from the expected manufacturing variability in the silicon layer.

Based on previously collected manufacturing variability data, we expect our silicon layer to vary in width from 470 – 510nm and in thickness from 215.3 – 223.1nm. We simulate the effective index over a range of 1500 – 1600nm for TE and TM polarization for the four corners of these ranges in Lumerical MODE, use MATLAB to extract the coefficients of the waveguide compact model in each case, and calculate the expected FSR. The ranges for all parameters are listed in the MIN and MAX columns in the tables below.

TE

	W 500, T 220	**W 470nm, T 223.1nm**	**W 510nm, T 223.1nm**	**W 510nm, T 215.3nm**	**W 470nm, T 215.3nm**	***MIN***	***MAX***
n1 (n_eff)	2.446821026	2.403880785	2.472208	2.441608	2.372449	2.372449	2.472208
n2	-1.133394603	-1.199155004	-1.10688	-1.121403	-1.213621	-1.21362	-1.10688
n3	-0.04393352	-0.045807142	-0.04516	-0.030738	-0.02507	-0.04581	-0.02507
n_g	4.203582661	4.26257104	4.187872	4.179782	4.253561	4.179782	4.262571

Mach-Zehnder Interferometer	**W 500, T 220**	**W 470nm, T 223.1nm**	**W 510nm, T 223.1nm**	**W 510nm, T 215.3nm**	**W 470nm, T 215.3nm**	***MIN***	***MAX***
FSR (nm) for ΔL=100um	5.715362808	5.6362697	5.736804	5.747908	5.648209	5.63627	5.747908
FSR (nm) for ΔL=200um	2.857681404	2.81813485	2.868402	2.873954	2.824104	2.818135	2.873954

Michelson Interferometer	**W 500, T 220**	**W 470nm, T 223.1nm**	**W 510nm, T 223.1nm**	**W 510nm, T 215.3nm**	**W 470nm, T 215.3nm**	***MIN***	***MAX***
FSR (nm) for ΔL=100um	2.857681404	2.81813485	2.868402	2.873954	2.824104	2.818135	2.873954

TM

	W 500, T 220	W 470nm, T 223.1nm	W 510nm, T 223.1nm	W 510nm, T 215.3nm	W 470nm, T 215.3nm	*MIN*	*MAX*
n1 (n_eff)	1.768820606	1.766348104	1.79625	1.74425	1.716673	1.716673	1.79625
n2	-1.258669838	-1.275269187	-1.316616	-1.187774	-1.136575	-1.31662	-1.13658
n3	1.91348782	1.969473507	1.85784	1.929451	1.995079	1.85784	1.995079
n_g	3.719758855	3.743015343	3.837004	3.5853	3.478364	3.478364	3.837004

Mach-Zehnder Interferometer	W 500, T 220	W 470nm, T 223.1nm	W 510nm, T 223.1nm	W 510nm, T 215.3nm	W 470nm, T 215.3nm	*MIN*	*MAX*
FSR (nm) for ΔL=100um	6.458752015	6.418621832	6.261396	6.700973	6.906982	6.261396	6.906982
FSR (nm) for ΔL=200um	3.229376008	3.209310916	3.130698	3.350486	3.453491	3.130698	3.453491

Michelson Interferometer	W 500, T 220	W 470nm, T 223.1nm	W 510nm, T 223.1nm	W 510nm, T 215.3nm	W 470nm, T 215.3nm	*MIN*	*MAX*
FSR (nm) for ΔL=100um	3.229376008	3.209310916	3.130698	3.350486	3.453491	3.130698	3.453491

Experiment Data

Below is the raw data measured for each of the TE interferometers. Unfortunately the TM interferometer data folders were empty, and the data could not be found.

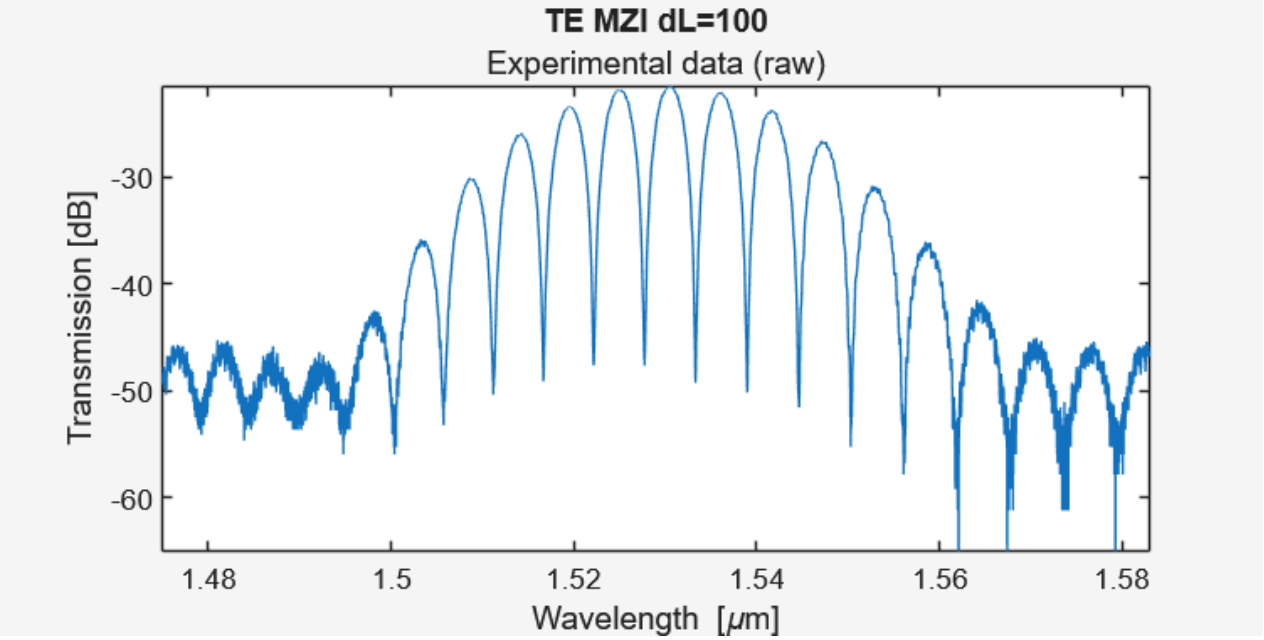

Figure 11: Measured interferometer transmission for the TE MZI with ΔL=100um

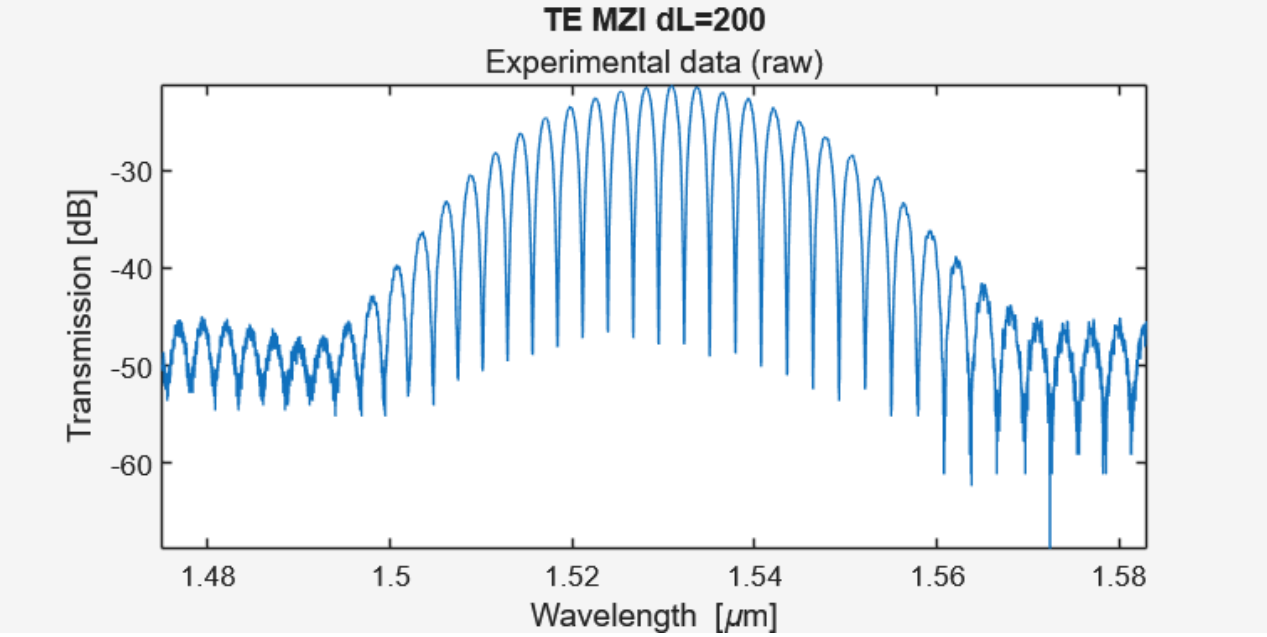

Figure 12: Measured interferometer transmission for the TE MZI with ΔL=200um

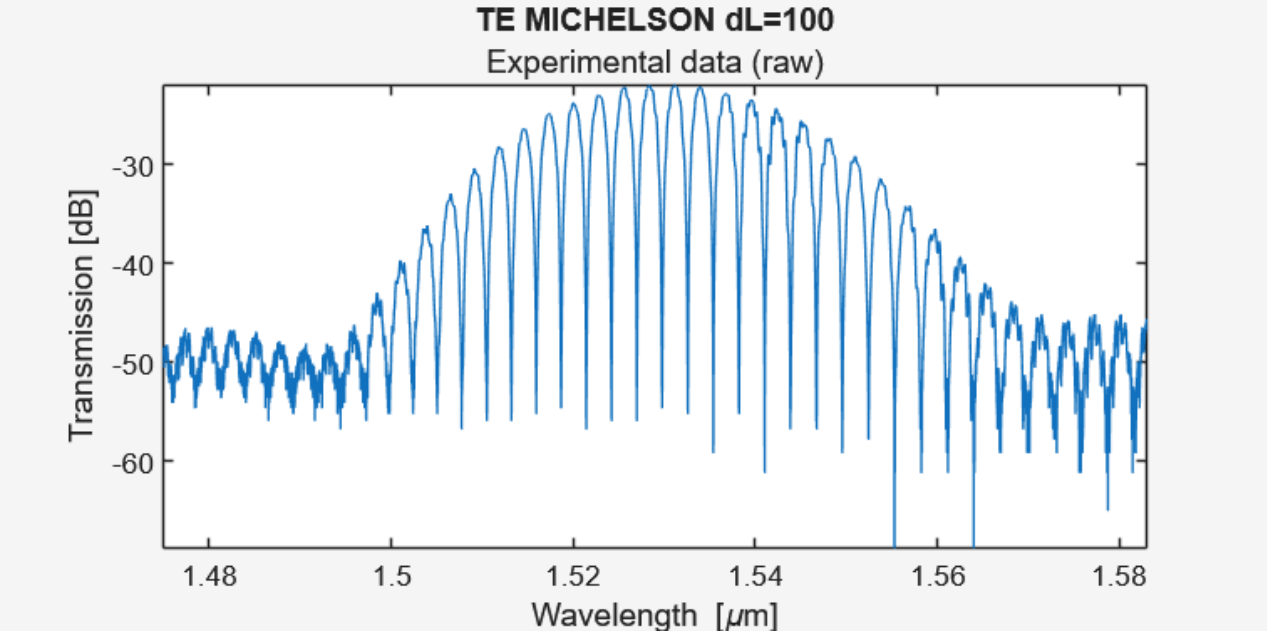

Figure 13: Measured interferometer transmission for the TE MICHELSON with ΔL=100um

Analysis

Now that we have our measured data, we can analyze it in order to find the group index and free-spectral range for each interferometer, and compare with the simulated results. For the sake of brevity in this report, we will show the entire data analysis process for just one of the interferometers; namely, the TE MZI with ΔL=100um. The same procedure has been applied to the data for the remaining interferometers and the results are summarized in the tables below.

Due to the limited bandwidth of the grating couplers, our spectra show a curved amplitude response. We can remove this curve by fitting the raw data with a low order polynomial (shown in figure 14) and subtracting it off (result shown in figure 15).

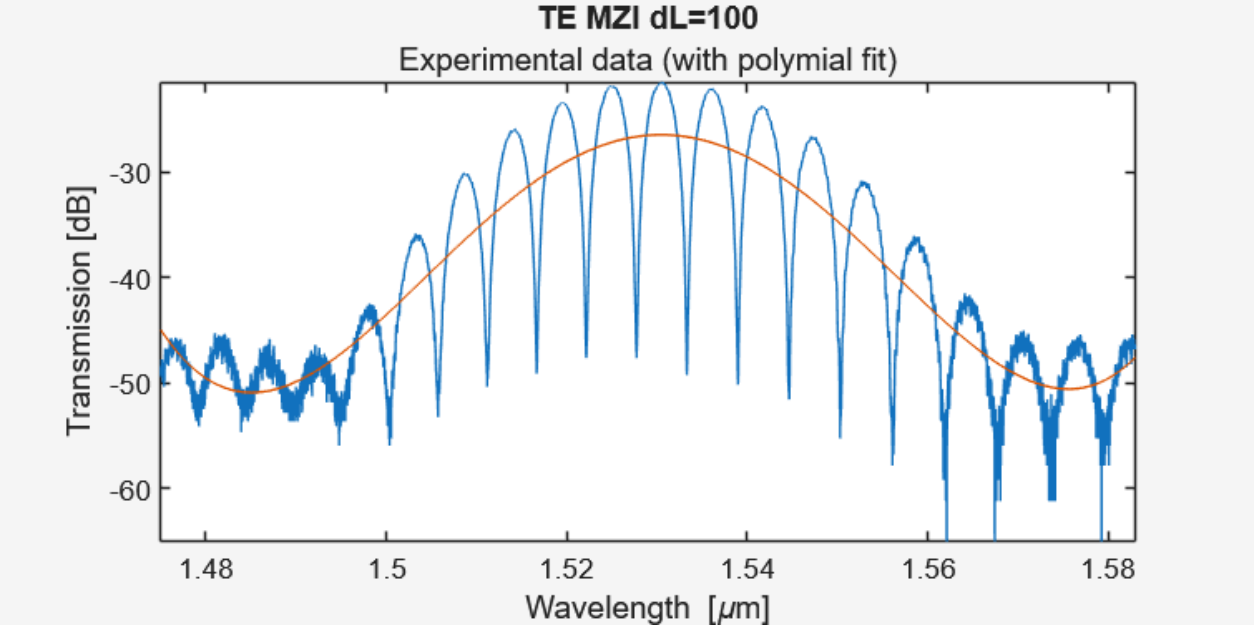

Figure 14: Experimental data with 4th order polynomial fit

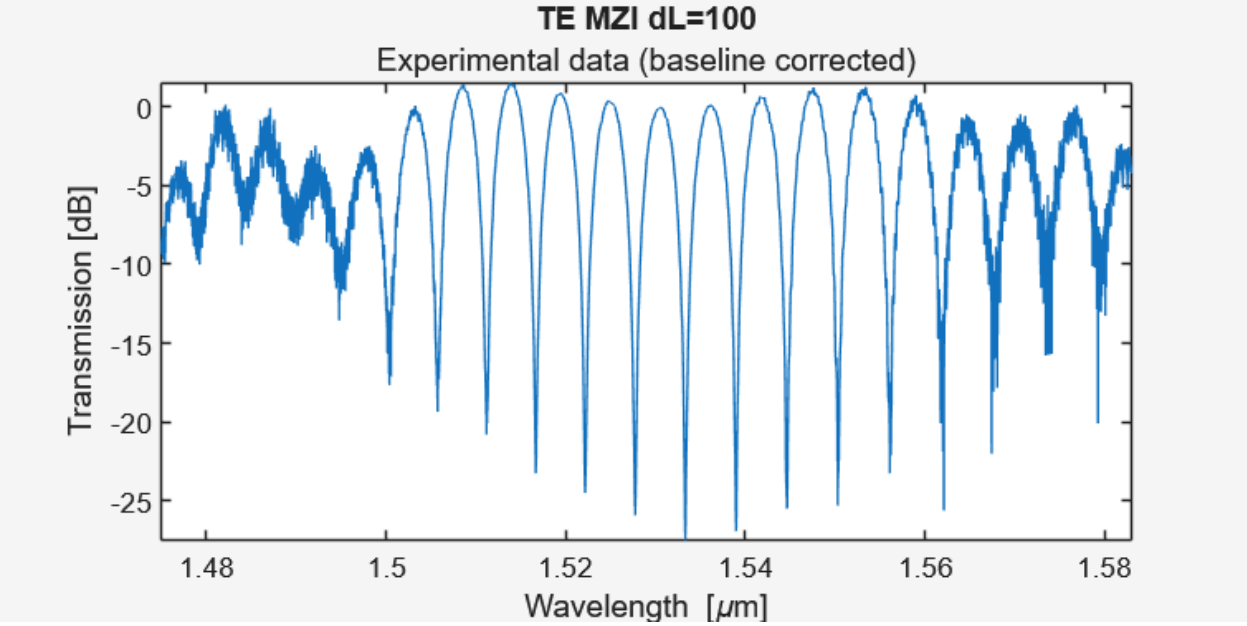

Figure 15: Experimental data corrected by subtracting 4th order polynomial fit from figure 13

Then, in order to avoid the noisy data at the edges of the spectra, we will trim our data to exclude points outside of 1.500 – 1.560 um (result shown in figure 16).

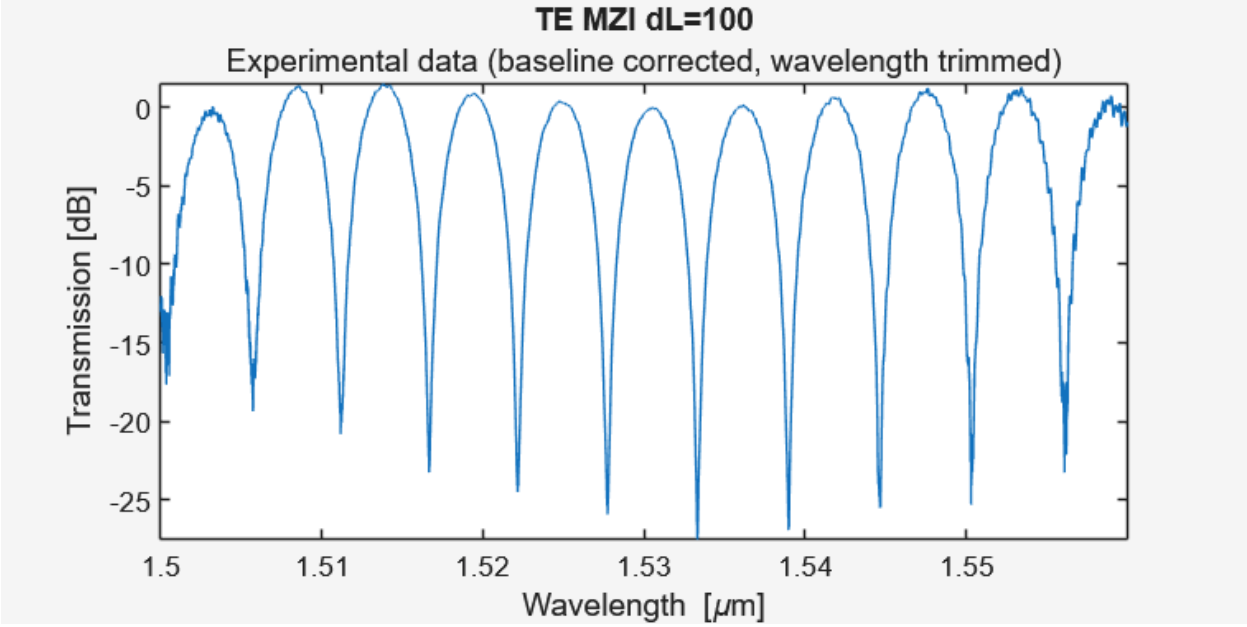

Figure 16: Curve corrected and wavelength trimmed data.

Next, we will programmatically generate the values of the theoretical MZI transfer function over our trimmed wavelength range and plot it over the measured data for comparison (show in figure 17).

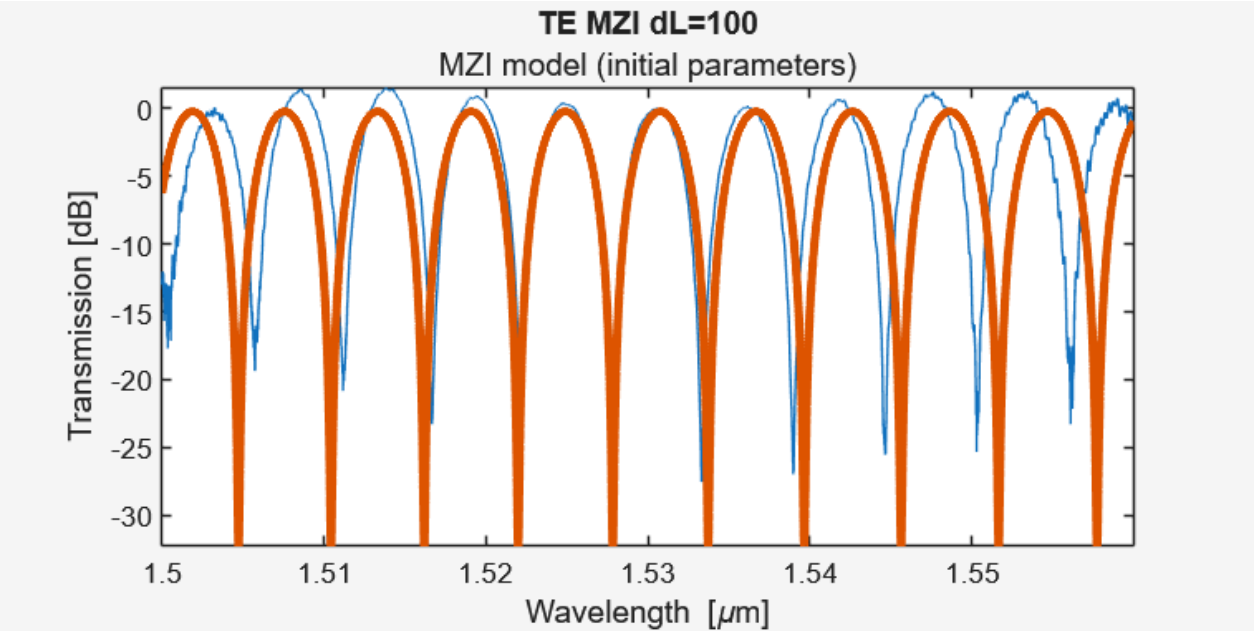

Figure 17: Theoretical transfer function overlayed on data

As expected (due to errors introduced by the manufacturing and measurement processes), the theoretical transfer function does not overlap the data perfectly. Therefore, we will optimize the parameters of the theoretical transfer function (using a least squares method) until we get a good fit with our measured data (result shown in figure 18).

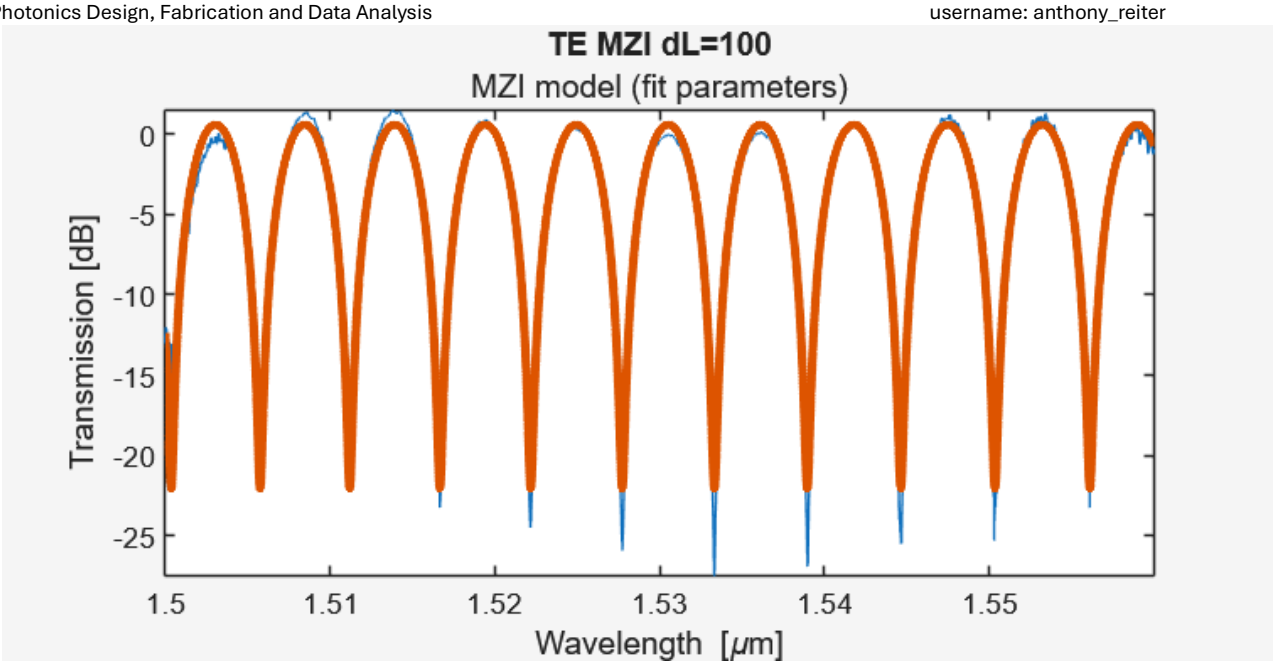

Figure 18: Optimized transfer function overlayed on data

We can use the parameters of this optimized transfer function to calculate the group index at each wavelength (result shown in figure 19).

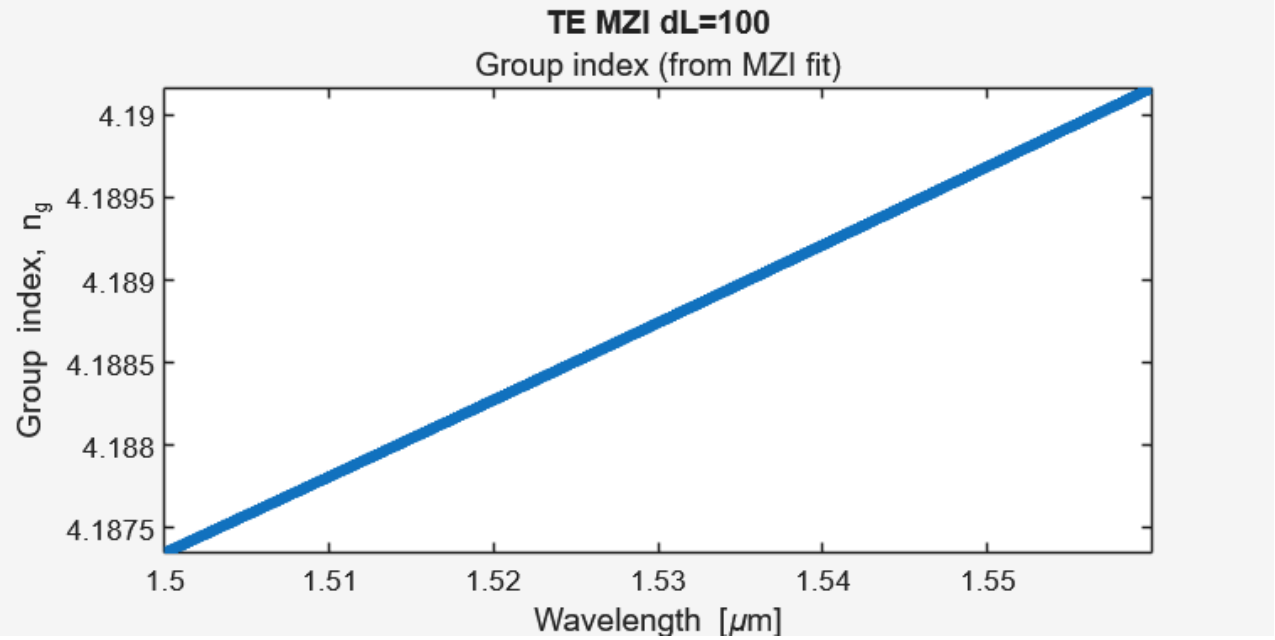

Figure 19: Group index data calculated from optimized transfer function

In order to determine the free spectral range of our device, we can find the coordinates of each peak (shown in figure 20) and directly subtract the wavelength span between them (result shown in figure 21).

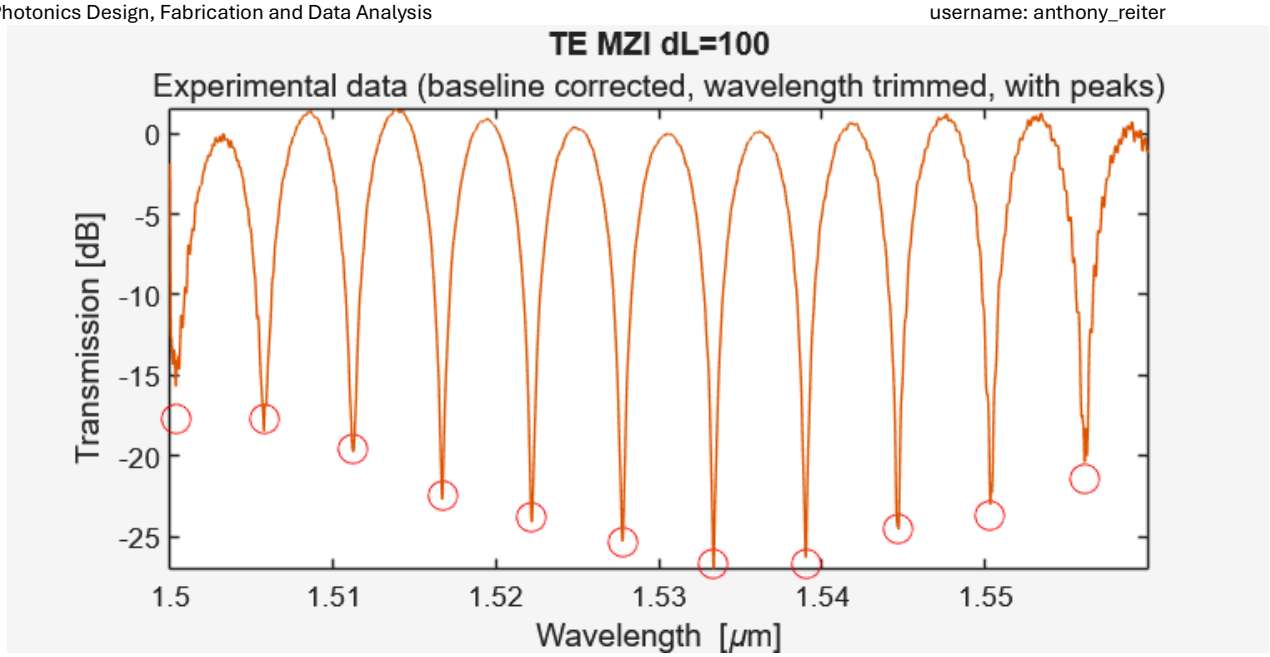

Figure 20: Identifying the peaks of our measured data

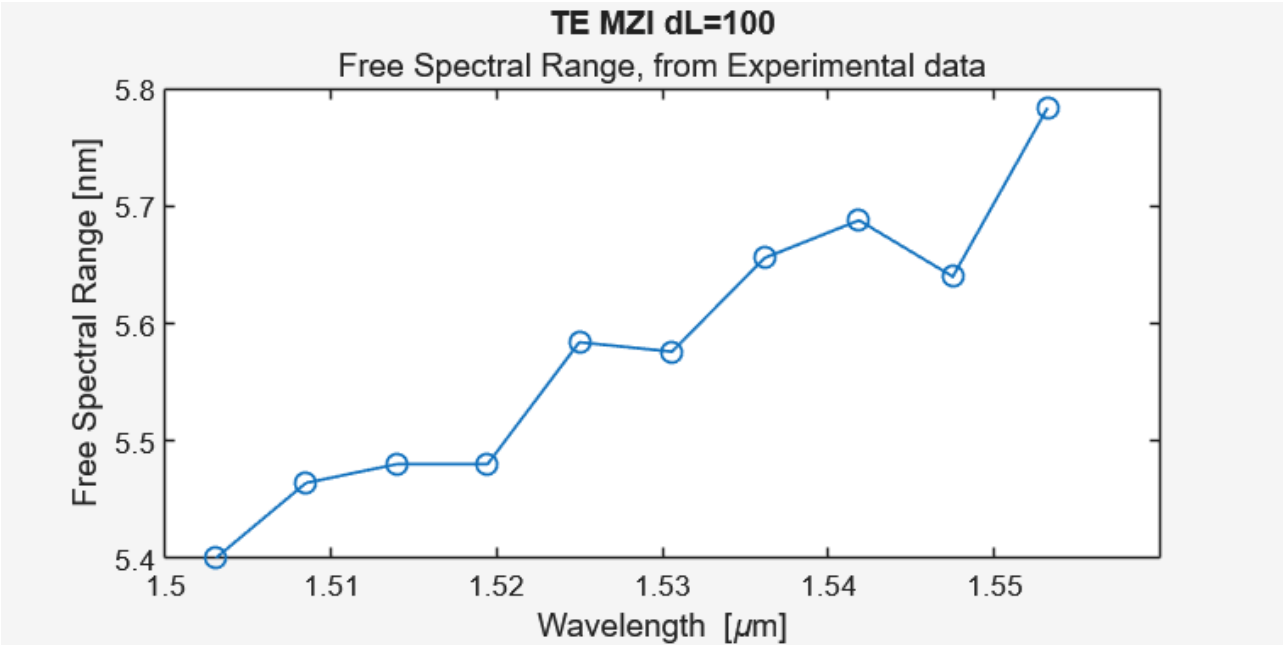

Figure 21: Free spectral range calculated from proximity of peaks in experimental data

TE

MZI ΔL=100um	Measured	Theoretical (nominal) r^2=0.9756	% difference	Theoretical (min from corner analysis)	Theoretical (max from corner analysis)
n1 (n_eff)	2.4494	2.446821026	-0.1	2.372449	2.472208
n_g	4.1887	4.203582661	0.4	4.179782	4.262571
FSR (nm)	5.64	5.715362808	1.3	5.63627	5.747908

MZI ΔL=200um	Measured	Theoretical (nominal) r^2=0.9800	% difference	Theoretical (min from corner analysis)	Theoretical (max from corner analysis)
n1 (n_eff)	2.4504	2.446821026	-0.1	2.372449	2.472208
n_g	4.1867	4.203582661	0.4	4.179782	4.262571
FSR (nm)	2.86	2.857681404	-0.1	2.818135	2.873954

MICHELSON ΔL=100um	Measured	Theoretical (nominal) r^2=0.9652	% difference	Theoretical (min from corner analysis)	Theoretical (max from corner analysis)
n1 (n_eff)	2.3977	2.446821026	2.0	2.372449	2.472208
n_g	4.1895	4.203582661	0.3	4.179782	4.262571
FSR (nm)	2.89	2.857681404	-1.1	2.818135	2.873954

Conclusion

In this work, we designed, simulated, fabricated, and experimentally characterized a series of silicon photonic Mach–Zehnder and Michelson interferometers with varying path length imbalances and polarizations. Using Lumerical MODE and INTERCONNECT, we established compact waveguide models, predicted the effective and group indices, and derived the corresponding free spectral ranges for each interferometer configuration. Fabrication variability (primarily arising from top silicon thickness and waveguide width deviations) was incorporated through a corner analysis, yielding realistic bounds for the expected optical behavior.

Experimental measurements of the TE-polarized interferometers showed strong agreement with simulated predictions. After baseline correction, wavelength trimming, and parameter optimization of the theoretical transfer function, the extracted group indices and FSR values closely matched both the nominal simulations and the ranges predicted by fabrication variability. In particular, we observed a maximum deviation of only 2% from theoretical expectations for the FSR, and the fitted group indices

remained well within the modeled bounds. Although TM data was unavailable, the consistency observed in the TE measurements demonstrates the robustness of the design methodology.

Overall, the results validate the accuracy of the compact waveguide models and confirm that even relatively simple interferometric structures enable reliable extraction of group index and dispersion-related parameters in silicon photonics. The close alignment between simulation and measurement highlights both the predictability of the fabrication platform and the effectiveness of the analytical tools used. These findings provide a solid foundation for further work involving more advanced interferometric architectures, dispersion engineering, and the integration of active components into silicon photonic circuits.

References

1. Lukas Chrostowski, Michael Hochberg. Silicon Photonics Design. Cambridge University Press (CUP), 2015.
2. Lukas Chrostowski, Michael Hochberg. Testing and packaging. 381–405 In Silicon Photonics Design. Cambridge University Press (CUP)
3. Yun Wang, Xu Wang, Jonas Flueckiger, Han Yun, Wei Shi, Richard Bojko, Nicolas A. F. Jaeger, Lukas Chrostowski. Focusing sub-wavelength grating couplers with low back reflections for rapid prototyping of silicon photonic circuits. Opt. Express 22, 20652 The Optical Society, 2014.
4. H. Subbaraman et al, ”Recent advances in silicon-based passive and active optical interconnects,” Opt. Express 23, 2487-2511 (2015)
5. K. Roberts et al, ”High Capacity Transport100G and Beyond,” Journal of Lightwave Technology , vol.33, no.3, pp.563,578, Feb.1, 1 2015
6. Y. Shoji et al, ”Low-crosstalk 2 2 thermo-optic switch with silicon wire waveguides,” Opt. Express 18, 9071-9075 (2010)
7. T. Li, E. Willner and I. Kaminow, ”Optical Fiber Telecommunications VA: Components and Subsystems,” Academic Press, 2010.
8. Lumerical MODE software. https://www.lumerical.com/tcad-products/mode/
9. Lumerical INTERCONNECT software. https://www.lumerical.com/tcad-products/interconnect/
10. Components library, SiEPIC, University of Washington. http://goo.gl/B9IRn8
11. KLayout software. http://www.klayout.de/